

# Stability of droplet-target laser-plasma soft x-ray sources

O. Hemberg,<sup>a)</sup> B. A. M. Hansson, M. Berglund, and H. M. Hertz

*Biomedical and X-Ray Physics, Royal Institute of Technology, SE-100 44 Stockholm, Sweden*

(Received 23 March 2000; accepted for publication 7 August 2000)

The spatial stability of microscopic target droplets used for laser-plasma soft x-ray generation in vacuum is investigated. A long-term drift in drop position is characterized with an ultrafast laser-diode imaging system. The drift is experimentally and theoretically shown to be due to a temperature-induced increase in target-liquid viscosity as a result of evaporation. Finally, the drift is compensated for and stable, long-term unattended operation of the source is demonstrated with an automatic phase-delay drop-to-laser synchronizing system. This is important for future compact lithography and microscopy systems. © 2000 American Institute of Physics. [S0021-8979(00)00822-7]

## I. INTRODUCTION

Laser-produced plasmas (LPP) are attractive soft x-ray and extreme ultraviolet (EUV) sources suitable for microscopy<sup>1</sup> and lithography.<sup>2</sup> Droplet-target laser-plasma sources are particularly interesting since they have been shown to reduce the debris production associated with traditional, bulk-target sources to almost negligible levels. However, droplet sources are sensitive to drift problems due to the necessity of accurate drop-to-laser synchronization. In this article we investigate the cause of this drift and the drop stability in general. Furthermore, the drift is successfully compensated for by a new automatic control system.

The debris created from LPPs consists of both ions and large atomic clusters.<sup>3</sup> There are several different methods to mitigate the effects of produced debris, including fast shutters,<sup>4</sup> gas shields,<sup>5</sup> foil traps, and rotating targets.<sup>6</sup> A more fundamental approach is to limit the amount of debris produced. Much work has been performed on different gas-target arrangements.<sup>2,7</sup> Using a size-optimized target we have previously shown negligible debris production using liquid jet<sup>8</sup> and liquid drop<sup>9-11</sup> targets while still retaining a high-density target. Furthermore, the droplet target and the liquid-jet sources are suitable for high-repetition-rate operation for high-average power, and grant nearly full,  $4\pi$  steradian, geometric access.

The liquid-droplet laser-plasma x-ray source does, however, suffer from a long-term drift, i.e., the drops move out of the laser focus in the direction of the drop path, which reduces the x-ray flux and may increase debris. This is a problem since unattended long-term operation is crucial for many applications. For liquids with certain hydrodynamic properties, including cryogenic liquids, this problem can be avoided using the liquid-jet target technique.<sup>8</sup> However, for conventional liquids, like water and ethanol, the high surface tension results in a drop-formation point close to the nozzle orifice, making it necessary to target individual drops since targeting the jet may result in nozzle damage. It is therefore important to stabilize the observed long-term drift. This ar-

ticle analyzes the drop stability in vacuum and actual droplet-based laser-plasma stability. Previous experimental work has concentrated on jet stability<sup>12-14</sup> and ink-jet applications<sup>15,16</sup> operating at atmospheric pressure with little regard to longitudinal stability. Work has also been performed on the stable production of larger cryogenic gas pellets for fusion and high-energy physics experiments.<sup>17,18</sup>

## II. BACKGROUND

The droplet-target laser-plasma x-ray source<sup>9,10</sup> has been described previously and is briefly summarized below. The experimental arrangement is shown in Fig. 1. Room-temperature liquid ethanol at a pressure of  $\sim 45$  bar (controlled by a standard gas governor attached to a 20 l, 200 bar tank) is injected into a vacuum chamber through a small, 10  $\mu\text{m}$  diameter, glass capillary nozzle piezoelectrically vibrated at  $\sim 1$  MHz (Siemans-Elena, Stockholm) giving  $\sim 10^6$  drops/s traveling at  $\sim 50$  m/s. A turbodrag pump, backed by a rotary-vane pump, is used to keep the vacuum pressure at  $\sim 10^{-5}$  mbar. To reduce the needed pump capacity a liquid-nitrogen cold trap is used to freeze excess ethanol. A 100 Hz frequency-doubled Nd:YAG laser (Coherent Infinity) with 3 ns long pulses of  $\sim 100$  mJ is used for plasma formation of the drops. The emission of laser pulses is synchronized to the piezoelectric drop-stimulating signal and a manually variable delay is used to adjust the phase so that each laser pulse hits a single drop. Since the drops are  $\sim 15$   $\mu\text{m}$  diameter and the laser focus only slightly larger, a laser focus and droplet overlap accuracy of a few microns is necessary.

A liquid jet is inherently unstable and will break up in a random manner due to the surface tension.<sup>19</sup> A small disturbance, random or applied, at the nozzle exit grows exponentially until drops are formed. The theoretical analysis of the fluid mechanics of liquid jets is more complex for viscous jets<sup>20</sup> than for nonviscous jets<sup>19</sup> but the results are similar. The time to breakup is longer for viscous jets but independent of jet speed in both cases. The distance  $L$ , to the drop formation point is<sup>14,15</sup>

$$L = 12v \left[ \sqrt{\frac{\rho d^3}{\sigma}} + \frac{3d\eta}{\sigma} \right], \quad (1)$$

<sup>a)</sup>Electronic mail: hemberg@physics.kth.se

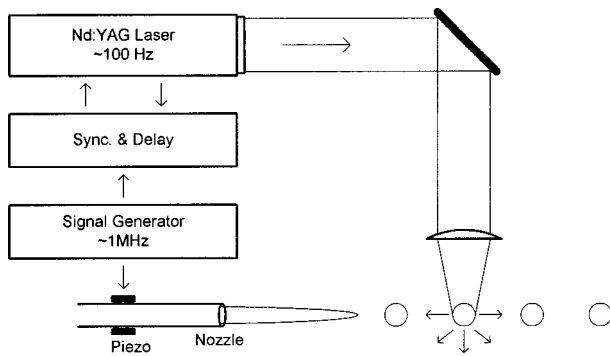


FIG. 1. Experimental arrangement of the droplet-target laser-plasma x-ray source.

where  $v$  is the jet speed,  $\rho$  is the density,  $\sigma$  is the surface tension,  $\eta$  is the viscosity, and  $d$  is the jet diameter. The drop diameter, is  $\sim 1.9$  times the jet diameter which is  $\sim 10\%$  smaller than the nozzle orifice. The average spontaneous drop formation frequency is<sup>14,15</sup>

$$f_r = \frac{v}{\lambda_m} = \frac{v}{4.5d}, \quad (2)$$

where  $\lambda_m$  is the drop separation distance. Since the spontaneous drop formation is stochastic, an external vibration is applied to simulate stable drop formation. For efficient drop stimulation the frequency of the applied vibration should be close to  $f_r$ . Furthermore, the flow must be laminar in order to form a stable jet. For conventional liquids this corresponds to a maximum Reynolds number  $R_e$  of  $\sim 1000$ , given by<sup>12</sup>

$$R_e = \frac{\rho v d}{\eta}. \quad (3)$$

For stable drop formation the right combination of all relevant parameters must be used. This has been thoroughly investigated by the ink-jet community and the stimulating frequency and amplitude found to be crucial.<sup>16</sup> For the remainder of this article a highly stable region of operation is assumed, i.e., small changes in parameters effect the drop formation but not the stability as such.

There are two types of instabilities that are of concern. First there are the microscopic drop-to-drop variations in size, speed, and direction. These will not be treated in detail, as Sec. III will show that they are sufficiently small for stable operation of the source. This article is instead focused on the slow, long-term drift.

Since the drops are targeted  $\sim 10$  mm away from the nozzle, a large variation in droplet position (at a specific time relative the stimulating frequency) is most likely caused by a variation in drop velocity. The jet speed is determined by the conversion of potential energy, given by the pressure, into kinetic energy in the capillary system. The pressure drop in a capillary system can be written as

$$\Delta p_{\text{tot}} = \Delta p_{\text{kin}} + \Delta p_{\text{visc}} + \Delta p_{\text{surf}} + \Delta p_{\text{loss}}, \quad (4)$$

i.e., the total pressure drop can be divided into a kinetic term, a viscous term, a surface tension term, and a term due to entrance and exit losses. Using the Hagen–Poiseuille<sup>21</sup> equation this can be written as

$$\Delta p_{\text{tot}} = \frac{1}{2} \rho v_0^2 + 32 \eta d_0^2 v_0 \int \frac{dl}{d^4(l)} + \frac{2\sigma}{d} + \Delta p_{\text{loss}}, \quad (5)$$

where  $v_0$  is the jet exit speed and  $d_0$  is the orifice diameter, and the integration is over the length,  $l$ , of the capillary. This equation may be solved to give the speed of the jet as a function of the pressure and the temperature, given a model for the viscosity's dependence of temperature. For ethanol, in the present temperature interval, the viscosity is modeled as

$$\eta = e^{A+B/(C-T)}, \quad (6)$$

where  $A$ ,  $B$ , and  $C$  are experimentally determined constants and  $T$  is the temperature.<sup>22</sup> Due to the  $d^4(l)$  term the solution is, however, very sensitive to the geometric modeling of the nozzle tip. By adjusting the model, excellent agreement with experimental data can be achieved, as shown in Sec. III. The speed's dependence of pressure and temperature is, however, independent of the geometric model of the nozzle. From Eqs. (5) and (6) it can be shown that roughly,

$$v \propto \sqrt{p} + \text{constant} \quad (7)$$

and

$$v \propto T + \text{constant} \quad (8)$$

for any realistic model of the nozzle geometry in our region of operation.

### III. EXPERIMENT AND DISCUSSION

In this section we experimentally measure and theoretically explain drop stability in vacuum in the absence of laser-plasma formation. This requires an imaging system yielding drop position with an accuracy of approximately  $1 \mu\text{m}$ .

There are several different methods to study drop stability. The most common is to use a synchronized stroboscopic light source. Since the resulting image is then made up of a large number of superimposed images, it is unsuitable for detailed drop stability analysis. Another method is to use a low-power continuous laser, crossing the drop path, and a photodiode to record the residual light.<sup>16</sup> This is unfortunately not suitable for long-term analysis nor can it be used to analyze stability in the directions perpendicular to the drop path. A better method is to have an ultrafast imaging system. Due to the size and speed of the drops, an exposure time of less than  $20$  ns is required for clear images ( $10\%$  motion blur). There are several different gated, image intensified systems capable of this, but they are often complex, expensive and usually suffer from image quality problems.

Instead of a short shutter time, an equally short laser pulse can be used as the single light source. The actual shutter time is then unimportant and standard CCD cameras may be used provided that the laser power is sufficient to allow single-shot exposures. The viability of this method has previously been demonstrated using a high-power Nd:YAG laser.<sup>16</sup> Figure 2 shows the system developed for the drop stability measurements in this article. It is based on a  $20$  mW,  $\lambda \approx 635$  nm laser diode emitting  $20$  ns pulses, a standard CCD equipped microscope and an image acquisition

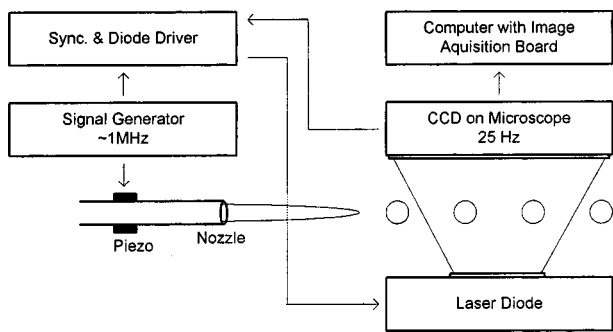


FIG. 2. Schematic view of the imaging system used for drop stability analysis.

board. Laser-diode illumination is advantageous compared to high-power laser illumination since it is more flexible in terms of pulse width, repetition rate, wavelength, and price. Because the CCD exposure time is  $\sim 10^5$  times longer than the laser illumination it is important to have 100% modulation of the laser diode to avoid integration of background light. In order to avoid split images due to the interlacing of standard CCDs, the laser pulse must first be synchronized to the camera. For frame-to-frame position analysis the laser pulse must also be synchronized to the drop-stimulating signal. The system is inexpensive compared to other solutions and has proven to be very useful.

The imaging system was used to record drop stability data  $\sim 10$  mm from the nozzle orifice. This distance corresponds to the typical distance between the laser plasma and the orifice during normal x-ray operation. A typical 20 ns single-shot exposure is shown in Fig. 3. The drop position was determined with an accuracy of  $0.5 \mu\text{m}$  by image analysis performed in MatLab. An edge detection filter used to define the perimeter of the drops and circles were then fitted to this edge data in order to determine the center positions.

All measurements were performed both in vacuum and in air at atmospheric pressure. First, the imaging system was operated at 25 Hz for 60 s, resulting in 1500 images for short-term stability analysis. Then the system recorded data at 1 Hz for 1–3.5 h giving 3600–12 600 images for long-term drift analysis. Short-term position stability was better for air operation but on the order of the measurement accuracy for both air and vacuum operation, both in the direction parallel and perpendicular to the drop path. During long-term operation the position stability perpendicular to the drop path did not change much and was better than  $1 \mu\text{m}$ . However, the long-term position drift parallel to the drop path was large, as shown in Fig. 4. In air the drift stabilizes after a few minutes while in vacuum the drift continues for hours. The

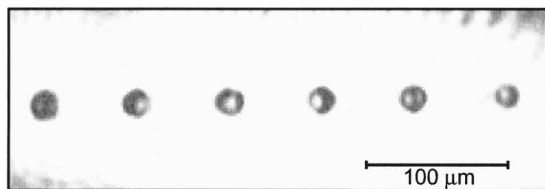


FIG. 3. Typical single-shot (20 ns) image of the drop train in midflight.

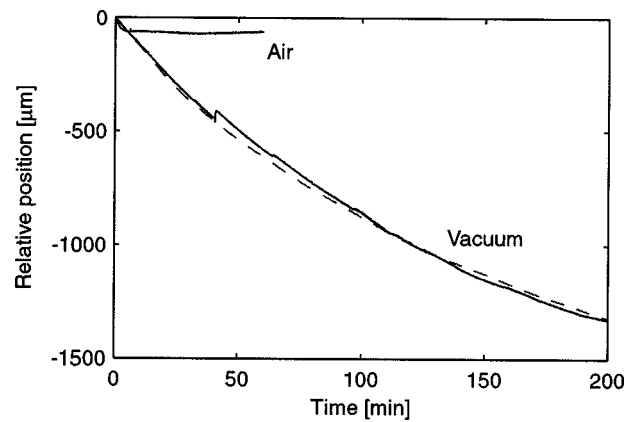


FIG. 4. Relative position of one droplet starting 8.5 mm from the nozzle tip. The drift is parallel to the drop path and shows a large difference in time constant for air and vacuum operation. The dashed curve shows the result of a theoretical calculation of the drift.

small, abrupt change in position shown in Fig. 4 (after approximately 40 min) is believed to be due to either a pressure related effect or a mode change in the drop formation due to the change in viscosity.

The long-term drift was assumed to be due to a change in pressure or in temperature. The pressure was quickly ruled out for a number of reasons. According to Eq. (7) the pressure change must be very large in order to produce the observed drift. Furthermore, a change in pressure does not account for the difference between vacuum and air operation. To confirm this, the gas governor was exchanged for a 20 l tank (40 bar) providing very stable pressure, but this did not influence the observed drift or stability.

In order to determine if a change in temperature could be the cause of the drift, the temperature of the capillary was measured during operation (four-wire measurement with a thin film Pt-100 sensor). The temperature was measured on the edge of a thin metal tube which protects the glass capillary. When operating in air, the temperature initially fell a few degrees and then stabilized. In vacuum, on the contrary, the change was significant as illustrated in Fig. 5.

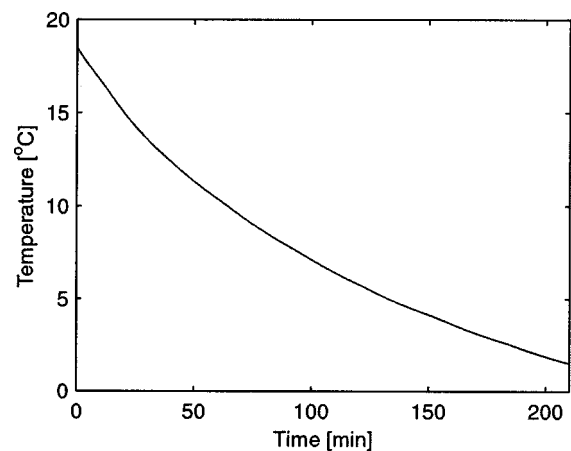


FIG. 5. Temperature of the nozzle as a function of time during vacuum operation.

The temperature curve of Fig. 5 is strikingly similar to the vacuum drift curve in Fig. 4. This agrees well with Eq. (8), stating that the speed is a linear function of the temperature in our region of operation. A quantitative calculation can be performed using a geometric model of the capillary nozzle and the full expression, given in Eqs. (5) and (6). Given the measured temperature data this results in the measured position as shown by the dashed line in Fig. 4, indicating good agreement between experiments and theory. Physically, the temperature decrease raises the viscosity of the liquid and therefore the speed also decreases, resulting in the observed position drift.

In order to positively identify the temperature as the cause of the drift, a small resistive heating device was attached to a capillary. When driving a current through the resistor a current-dependent velocity drift was induced. From this experiment and the drift/temperature similarities, the temperature is identified as the major cause of the drift.

When the liquid leaves the orifice it immediately starts to evaporate. The evaporation causes a net cooling effect on the capillary and the liquid. The difference between the atmospheric case and the vacuum case is the rate of evaporation and the heat transfer. In vacuum, the net rate of evaporation is higher, producing more cooling power. When operating at atmospheric pressure the air surrounding the capillary acts as a heat conductor, quickly stabilizing the system. When operating in vacuum, heat transfer is limited to radiation, and to conduction through the nozzle encapsulations and fittings. This results in less heat conduction, resulting in the much longer thermal time constant of the system.

#### IV. STABILIZATION

In this section the described longitudinal drop drift in the droplet-target laser-plasma source is compensated for by a feedback system, making long-term unattended stable x-ray generation possible. The original experimental arrangement was described in Sec. II. Here a 100 Hz frequency-doubled Nd:YAG laser (Coherent Infinity) with 3 ns long pulses of  $\sim 100$  mJ is synchronized to the  $\sim 1$  MHz piezoelectric drop-stimulating frequency. When the laser is ready to fire, the synchronization electronics waits for the drop clock and then sends a signal to the laser  $Q$ -switch, triggering the laser pulse emission. A manually variable delay, in the signal path, is used to adjust the laser pulse emission time so that a single drop is hit. Although simple and straightforward, this method is sensitive to changes in drop position and the delay system must be supervised and manually tuned to compensate for the evaporation-induced drift in drop position. Initial attempts were made to stabilize the temperature of the nozzle and thus remove the drift. This was not very successful since it requires very accurate temperature control of the liquid inside the nozzle. Therefore an automatic control system based on feedback from the laser plasma was designed. This approach has the advantage that it compensates for any minor causes of change in the drop position, in addition to the major evaporation-induced temperature and viscosity drift discussed above.

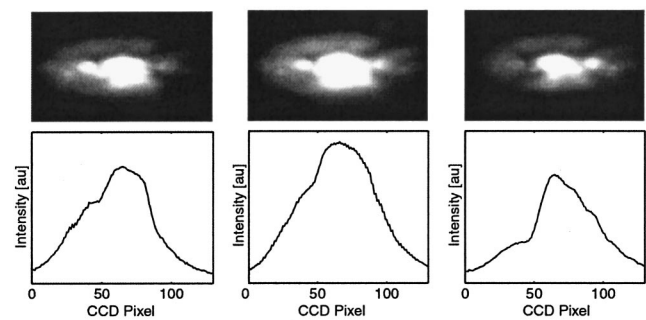


FIG. 6. Typical plasma images and intensity distributions used by the automatic phase-control system.

The feedback signal is derived from visible-wavelength images of the laser plasma recorded asynchronously by a standard CCD camera attached to a microscope and an image acquisition board. Scattered green light is eliminated with a filter (OG590). To reduce interlace problems several images are averaged. Figure 6 shows three representative images for when the laser pulse is fired somewhat too early (left-hand side), correct (mid), or somewhat too late (right-hand side). Using the fact that the intensity distribution should be symmetric and centered when correctly targeting an individual drop, the system is able to maintain spatial and temporal synchronization of the laser and the drop target by continuously adjusting the phase delay of the control electronics described in the next paragraph. Simply monitoring the x-ray flux from the source is not sufficient since it does not give information on whether to increase or decrease the phase delay.

A schematic of the new automatic control electronics is shown in Fig. 7. It does not use a delay but rather a phase shift to synchronize the laser and the drops. The signal generator used for drop formation (SRS DS345) is now also used as a reference to phase lock an additional signal generator (AD9830) with the same frequency as the drop generator. When the laser is ready to fire, the system now waits for the signal from the second generator before sending the trig signal to the  $Q$ -switch. Since the phase of the second

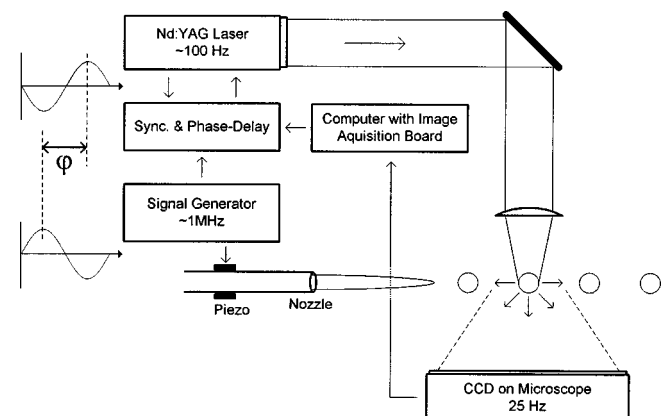


FIG. 7. Schematic view of the new automatic control system and trigger electronics. The CCD camera monitors plasma symmetry in the visible wavelength region and the computer controls the phase shift,  $\phi$ , to compensate for any drift.

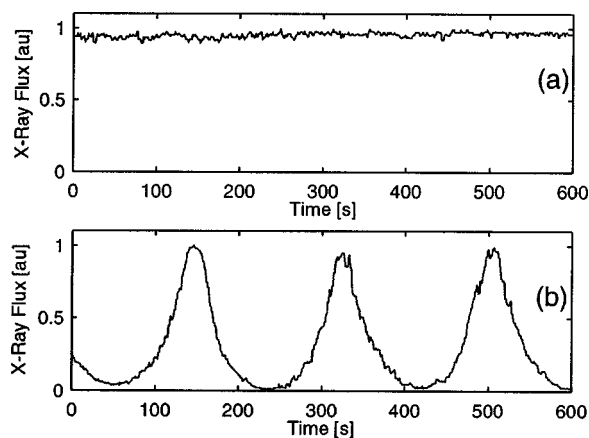


FIG. 8. X-ray flux as a function of time, with (a) and without (b) the automatic control system active.

generator is digitally programmable (12 bit), the relative phase,  $\varphi(0-2\pi)$ , between the laser and drop train can now be controlled in a very accurate manner. This phase-delay approach eliminates much of the problem with a highly stable, long temporal delay that has to be reset to zero when exceeding one drop period. Due to the cyclic nature of the phase delay there will be no abrupt change when the delay exceeds one drop period since a phase delay of  $2\pi + \delta$  behaves just like a phase delay of  $\delta$ , only now on the next drop.

The first version of the control system only uses a proportional control algorithm and a crude algorithm to determine the plasma center position. Although this can be improved, the effect of the current system is clearly shown in Fig. 8, where x-ray flux is plotted as a function of time with (a) and without (b) the system active. The x-ray flux was measured with a GaAsP diode (Hamamatsu G1127-02) and the data points in Fig. 8 are 1 s averages. The diode was covered by a 100 nm Ag/160 nm Al sandwich filter, which predominantly transmits highly ionized carbon emission around  $\lambda = 3-4$  nm. When the system is not active, the individual passing of drops as they drift in and out of the laser focus is clearly observable. With the system active, long-term stable unattended operation of the droplet-target laser-plasma source is demonstrated. As can be seen in Fig. 8, the phase correction necessary to compensate for the drift is initially around  $\pi$  per minute since two consecutive peaks represent one full period. With time, the required phase correction decreases since the magnitude of the drift decreases, as shown in Fig. 5.

The response time of the current system is  $\sim 1$  s, which is more than enough to correct for the observed drift. It is however only limited by the slow, asynchronous image acquisition. Principally, the system can be operated well above 10 kHz, given synchronized, high-speed image acquisition and data processing. Furthermore, the control system assumes hydrodynamic directional stability of the jet perpendicular to the drop direction and only stabilizes the phase of

the droplets, i.e., only compensates for drift parallel with the drop direction. With the nozzles used in this experiment we have noticed minute directional instabilities not previously observed. This directional instability, which occurs only in the presence of laser-plasma operation, is not yet fully understood.

## V. SUMMARY

The spatial and temporal stability of a droplet-target laser-plasma soft x-ray source has been investigated, with emphasis on long-term behavior. The short-term drop-to-drop position variation was experimentally determined to be small enough for stable operation of the source. A long-term drift in the longitudinal drop position has been found to be primarily due a temperature-induced change in the viscosity due to evaporation cooling of the nozzle. A new automatic control system monitoring plasma symmetry compensates for this and other long-term drifts. With this system the source may be operated unattended for long periods, which is crucial in many applications.

## ACKNOWLEDGMENTS

The authors are in debt to G. Johansson for fruitful discussions and M. Hemberg for invaluable electronic design support. This work was funded by the Swedish National Board for Industrial Development and the Swedish Engineering Science Research Council.

- <sup>1</sup>M. Berglund, L. Rymell, M. Peuker, T. Wilhein, and H. M. Hertz, *J. Microsc.* **197**, 268 (2000).
- <sup>2</sup>G. D. Kubiak, L. J. Bernardez, K. D. Krenz, D. J. O'Connell, R. Gutowski, and A. M. M. Todd, *OSA Trends Opt. Photonics Ser.* **4**, 66 (1996).
- <sup>3</sup>R. Bobkowski and R. Fedosejevs, *J. Vac. Sci. Technol. B* **14**, 1973 (1996).
- <sup>4</sup>A. L. Hoffman, G. F. Albrecht, and E. A. Crawford, *J. Vac. Sci. Technol. B* **3**, 258 (1985).
- <sup>5</sup>D. J. Nagel, *Microelectron. Eng.* **3**, 557 (1985).
- <sup>6</sup>L. A. Shmaenok, C. C. de Bruijn, H. Fledderus, R. Stuijk, A. A. Schmidt, D. M. Simanovskii, A. A. Sorokin, T. A. Andreeva, and F. Bijkerk, *Proc. SPIE* **3331**, 90 (1998).
- <sup>7</sup>H. Fiedorowicz, A. Bartnik, Z. Patron, and P. Parys, *Appl. Phys. Lett.* **62**, 2778 (1993).
- <sup>8</sup>L. Malmqvist, L. Rymell, M. Berglund, and H. M. Hertz, *Rev. Sci. Instrum.* **67**, 4150 (1996).
- <sup>9</sup>L. Rymell and H. M. Hertz, *Opt. Commun.* **103**, 105 (1993).
- <sup>10</sup>H. M. Hertz, L. Rymell, M. Berglund, and L. Malmqvist, *Proc. SPIE* **2523**, 88 (1995).
- <sup>11</sup>L. Rymell, M. Berglund, and H. M. Hertz, *Appl. Phys. Lett.* **66**, 2625 (1995).
- <sup>12</sup>R. E. Phinney, *AIChE J.* **18**, 432 (1972).
- <sup>13</sup>R. W. Fenn and S. Middleman, *AIChE J.* **15**, 379 (1969).
- <sup>14</sup>M. J. McCarthy and N. A. Molloy, *Chem. Eng.* **7**, 1 (1974).
- <sup>15</sup>J. Heinzl and C. H. Hertz, *Adv. Electron. Electron Phys.* **65**, 91 (1985).
- <sup>16</sup>L. Palm and J. Nilsson, *J. Imaging Sci. Technol.* **41**, 48 (1997).
- <sup>17</sup>C. A. Foster, K. Kim, R. J. Turnbull, and C. D. Hendricks, *Rev. Sci. Instrum.* **48**, 625 (1977).
- <sup>18</sup>B. Trostell, *Nucl. Instrum. Methods Phys. Res. A* **362**, 41 (1995).
- <sup>19</sup>J. S. W. Rayleigh, *Proc. London Math. Soc.* **10**, 4 (1879).
- <sup>20</sup>C. Weber, *Z. Angew. Math. Mech.* **11**, 136 (1931).
- <sup>21</sup>See, e.g., J. F. Douglas, J. M. Gasiorek, and J. A. Swaffield, *Fluid Mechanics*, 3rd ed. (Longman Scientific, Harlow, 1995), p. 296.
- <sup>22</sup>D. S. Viswanath and G. Natarajan, *Data Book on the Viscosity of Liquids* (Hemisphere, New York, 1989), p. 295.